Enhanced High-Temperature Energy Storage in Semi-Aromatic Polyimides via Dual Regulation of Short-range Ordered and Crosslinked Architectures

Guanghu He, Hang Luo*, Yuan Liu, Yuting Wan, Bo Peng, Deng Hu, Fan Wang, Xiaona Li, Jiajun Peng, Huan Wang, Dou Zhang*

State Key Laboratory of Powder Metallurgy, Central South University, Changsha 410083, Hunan Province, P. R. China

E-mail: hangluo@csu.edu.cn (H. Luo), dzhang@csu.edu.cn (D. Zhang)

Experimental Section

1. Materials

To minimize errors introduced during the purification process, all monomers were sourced from TCI (Shanghai) Chemical Industry Development Co., Ltd., including dodecahydro-[5,5'-biisobenzofuran]-1,1',3,3'-tetraone (>97.0% (T)), 4,4'-methylenedianiline (>98.0% (T)), and 4,4'-methylenebis(2-ethylaniline) (>98.0% (T)). N-methyl-2-pyrrolidone (NMP, analytical grade, ≥99.0%) was procured from Sinopharm Chemical Reagent Co., Ltd. Both the commercial BOPP and PEI were purchased from Polyk.

2. Synthesis of semi-aromatic polyimide film

2.1 Synthesis of semi-aromatic polyimide film in air

The dianhydride and diamine are copolymerized in equimolar ratios, and the reaction environment is maintained dry using a desiccator. The synthesis process of SAPI and E-SAPI and the film preparation process are shown in Figure S1. Initially, the diamine is dissolved in NMP, followed by the addition of the equimolar dianhydride. The mixture is tightly sealed and allowed to react for 12 hours, followed by thermal imidization. According to the experimental protocol, the thermal imidization in the air for $SAPI_{230}$ and $E\text{-}SAPI_{230}$ is conducted at 70 °C for 2 hours, 190°C for 2 hours, and 230 °C for 1 hour. For $SAPI_{260}$ and $E\text{-}SAPI_{260}$, the imidization procedures in the air are 70°C for 2 hours, 190°C for 2 hours, and 260°C for 1 hour. . For $SAPI_{290}$ and $E\text{-}SAPI_{290}$, the thermal imidization in the air follows the schedule of 70 °C for 2 hours, 190 °C for 2 hours, and 290 °C for 1 hour.

2.2 Synthesis of semi-aromatic polyimide film in vacuum

All sample synthesis steps in the vacuum are basically the same as in the air.

3. Characterization

3.1 Basic structure characterization

Attenuated total reflection Fourier-transform infrared (ATR-FTIR) spectroscopy was performed with a Nicolet 6700 instrument over the range of 4000~600 cm^{-1} to determine the functionalization of the samples. Imidization degree (ID), the film was treated at 290℃ as a 100% imidization object, and the relative imidization degree of other samples was calculated by

$$ID = \frac{(\frac{A_{1376}}{A_{1500}})_x}{(\frac{A_{1376}}{A_{1500}})_{290}}$$

where A represented the integral area of the peak and x represented the imidization treatment temperature.

Using the Shimadzu (XPS, X-ray Photoelectron Spectroscopy) instrument, the C, N, and O elements in SAPI and E-SAPI samples were analyzed.

Differential scanning calorimetry (DSC) thermograms of the polymers were obtained by a TA Q10 DSC instrument under a nitrogen atmosphere at the 5 °C/min scanning rate.

The powder 1D WAXD experiment was conducted on the Japanese Rigu Smartlab SE Panaco advance diffractometer with 40 kV FL (Cu Ka) and LYNXEYE_XE detectors as X-ray sources. The scanning speed of WAXD 1D is 5 °/min, scanning range from 5° to 40°. The values of the d-spacing were determined based on Bragg's law.

$$d = \frac{\lambda}{2sin\theta}$$

The Wide-Angle X-ray Scattering (WAXS) instrument (Anton Paar brand, Cu-target model) operates with a voltage not exceeding 40 kV and a current not exceeding 50 mA, with a scattering vector q range of 0.07 to 28 nm^{-1}.

Thermogravimetric analysis (TGA) of the polymers was performed on a TA SDT 2960 instrument at a heating rate of 10 °C/min in a nitrogen atmosphere.

UV-Vis-NIR absorption spectra of the thin polymer films about 10 μm were tested by Shimadzu UV-3600 plus spectrometer.

3.2 Electrical characterization

Young's modulus (Y) was measured using a nanomechanical testing system (MML, NanoTest Vantag, Britain) at a Poisson's ratio of 0.3. When subjected to electric fields, polymer dielectrics undergo a modulation in their Y due to the influence of electrostatic forces and temperature, thereby instigating localized stress concentrations within the material. These stress concentrations precipitate micro-wave formation, whose propagation, under the combined influence of electrostatic and mechanical stresses, facilitates the gradual expansion of micro-cracks, culminating in electromechanical breakdown (E_{em}).

$$(E_{em} = 0.606\sqrt{\frac{Y}{\varepsilon_0 \varepsilon_r}})$$

The films electrical studies used the films with Au electrodes of 3/8 mm in diameter. The temperature-dependent dielectric constant and dielectric loss of the polymers were measured using the BALAB DMS-500 with a frequency range from 40 Hz to 1 MHz. The dielectric constant is calculated by

$$\varepsilon_r = \frac{Cd}{\varepsilon_0 A}$$

where A is the electrode area, ε_0 is the dielectric constant of the vacuum (8.85×10^{-12} F/m), C is the capacitance, and d is the thickness of the film. The polarization-electric field hysteresis loops of the polymer were obtained at 100 Hz by a TF analyzer 3000 ferroelectric polarization tester (aixACT, Germany). Twenty-one circular gold electrodes with an area of 7.065 mm^2 were provided for 3 × 3 cm thin film samples by magnetron sputtering, and the voltage ramp rate of the P-E curve test of all samples was 10 MV/m. The energy storage performance was calculated according to the P-E loops. Double-parameter Weibull statistics were conducted on the E_b of polymer film

according to equation

$$P(E) = 1 - exp\left[-\left(\frac{E}{E_b}\right)^{\beta}\right]$$

where E is the applied electric field, β is the shape parameter and E_b is the breakdown strength when the cumulative failure probability [P(E)] is 63.2%. As an index to evaluate the energy storage performance, the energy density (U) and efficiency (η) values are obtained by

$$U = \int E dD$$

$$\eta = \frac{U_d}{U_c},$$

where D represents the electric displacement and D is equal to P when ε_r>1, U_c represents the charging energy density and U_d is the discharge energy density. The current density of hopping conduction is *J*,

$$J = 2nq\lambda v exp\left(-\frac{\mu_H}{k_B T}\right) \sinh\left(\frac{q\lambda E}{2k_B T}\right)$$

where λ is mean hopping distance, *n* is carrier concentrations in the conduction band, *v* is the thermal vibration frequency of trapped carriers, E_a is activation energy from traps to the bottom of the conduction band, μ_H is the barrier height, *q* is the electronic charge, *E* is the electric field and k_B is the Boltzmann's constant.

The pulse discharge performance was tested by the dielectric material charge measurement system (DCQ-20A, PolyK Technologies, USA). The energy density of pulse discharge can be defined by

$$W_d = R\int I^2(t)dt/V$$

where W_d, R, I, T and V represent pulse discharge energy density, load resistance (R=10 kΩ), current, discharge time and sample volume, respectively.

3.3 Quantum chemical calculations

The geometry optimization was performed using density functional theory (DFT)/B3LYP/6-31G(d), with the int=ultrafine parameter employed to enhance computational accuracy. Subsequently, bandgap and electrostatic potential visualizations were conducted using Multiwfn and VMD software. The dihedral angle quantification benefited from a small program provided by Sobereva. The electron-hole method is used to look at the distribution of electron-holes and what happens when ethyl is introduced all calculations were carried out using Gaussian 16 software. One of the key indices used is the average distance D, which quantifies the spatial separation between the electron and hole distributions. This index provides a more nuanced view of charge transfer properties in the excited state. The formula for D is given by

$$\mathrm{D} = \sqrt{(x_{ele} - x_{hole})^2 + (y_{ele} - y_{hole})^2 + (z_{ele} - z_{hole})^2}$$

helps identify the extent of charge transfer within the molecule. where $(x_{ele}, y_{ele}, z_{ele})$ and $(x_{hole}, y_{hole}, z_{hole})$ are the coordinates of the electron and hole distributions, respectively, and the angle brackets denote averaging over the entire spatial distribution.

A larger DDD value indicates a more extensive separation, signifying a more pronounced charge transfer in the system.

The interaction strength is quantified by

$$S_r = \int S_r(r)dr = \int \sqrt{\rho^{hole}(r)\rho^{ele}(r)}\, dr$$

where ρ^{hole} is the hole distribution, representing the spatial regions where electron density is missing, ρ^{ele} is the electron distribution, indicating where electrons accumulate after excitation and r is the coordinate vector. This index quantifies the overlap between these distributions, with a higher S_r suggesting stronger interaction between the electron and hole.

To account for spatial correlation effects, the correlation index H is introduced, and the corrected separation is calculated as

$$t = D - H_{CT}$$

where H_{CT} is the spatial correlation component. A smaller t suggests a more significant overlap between the charges. The Coulomb interaction energy,

$$\mathrm{E}_C = \iint \frac{\rho^{hole}(r)\rho^{ele}(r)}{r_1 - r_2}\mathrm{d}r_1\mathrm{d}r_2$$

provides insights into the binding force between electrons and holes, with a higher value indicating stronger coupling. The spatial extent of the distributions is further described by the Hole Delocalization Index (HDI) and Electron Delocalization Index (EDI), calculated as,

$$HDI = 100 \times \sqrt{[\rho^{hole}(r)]^2 dr}$$

$$EDI = 100 \times \sqrt{[\rho^{ele}(r)]^2 dr}$$

respectively. The smaller the HDI (or EDI) value, the higher the degree of hole (or electron) delocalization, meaning the distribution is more uniform and spread out. These indices collectively form a comprehensive framework for assessing the spatial characteristics, interaction strength, and charge transfer dynamics in materials.

Additionally, the occupied and free volumes of SAPI and E-SAPI were calculated using Materials Studio 2020, while the geometric optimization of the monomer was performed with the COMPASS force field. 10 PI chains with each one containing 25 repeat units were packed into a periodic box for the amorphous cell construction with an initial density of 0.1 g/cm^3. FFV is calculated based on the equation

$$FFV = \frac{V_f}{V_t}$$

where V_f is the free volume and V_t is the total volume.

Table S1. Excitation characteristics (D, Sr, H), excitation energy (E_{ee}), exciton binding energy (Coulomb attractive energy, E_{coul}), hole delocalization index (HDI) and electron delocalization index (EDI) of SAPI by TD-DFT calculated.

State	D (Å)	S_r	H (Å)	E_{ee} (eV)	E_{coul} (eV)	HDI	EDI
S_1	0.20	0.55	2.57	4.89	5.74	17.12	12.04
S_2	0.28	0.53	2.47	4.89	5.72	18.19	12.61
S_3	0.26	0.54	2.63	4.91	5.44	17.51	12.12
S_4	0.26	0.54	2.58	4.91	5.83	17.60	12.22
S_5	0.21	0.55	2.60	5.17	5.63	16.88	11.24

Table S2. Excitation characteristics (D, Sr, H), excitation energy (E_{ee}), exciton binding energy (Coulomb attractive energy, Ecoul), hole delocalization index (HDI) and electron delocalization index (EDI) of E-SAPI by TD-DFT calculated

State	D (Å)	S_r	H (Å)	E_{ee} (eV)	E_{coul} (eV)	HDI	EDI
S_1	0.26	0.54	2.54	4.91	5.78	16.95	12.10
S_2	0.24	0.54	2.57	4.92	5.62	17.01	12.14
S_3	0.28	0.54	2.50	4.92	5.63	17.09	12.26
S_4	0.25	0.53	2.38	4.93	6.01	17.93	12.47
S_5	0.15	0.56	2.68	5.29	5.38	15.92	10.73

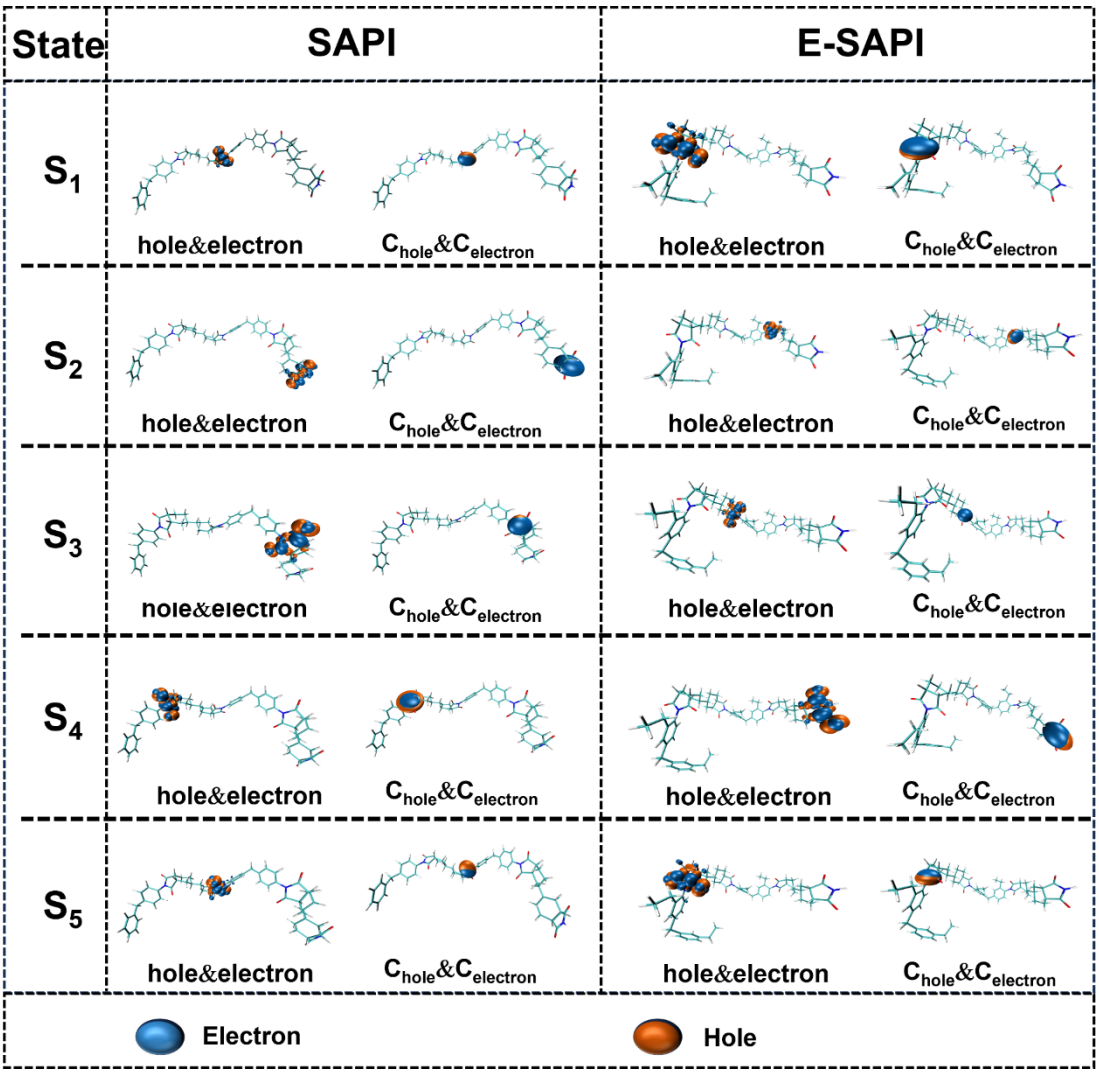

Figure S1. The electron-hole diagrams and Chole-Cele diagrams of SAPI and E-SAPI by TD-DFT (Time-Dependent Density Functional Theory) were calculated.

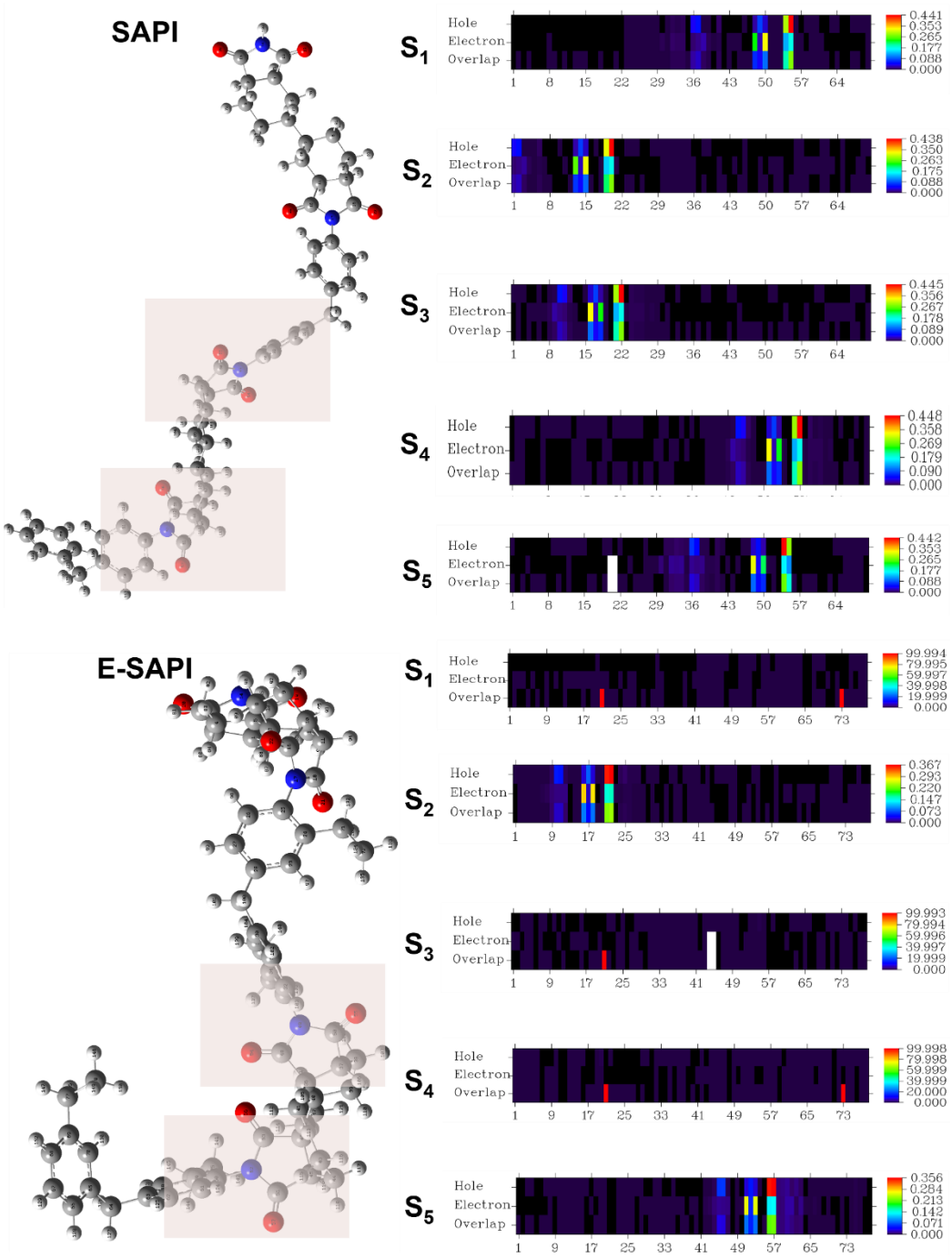

Figure S2. SAPI and E-SAPI heat maps obtained by fragment-contribution hole and electron methods.

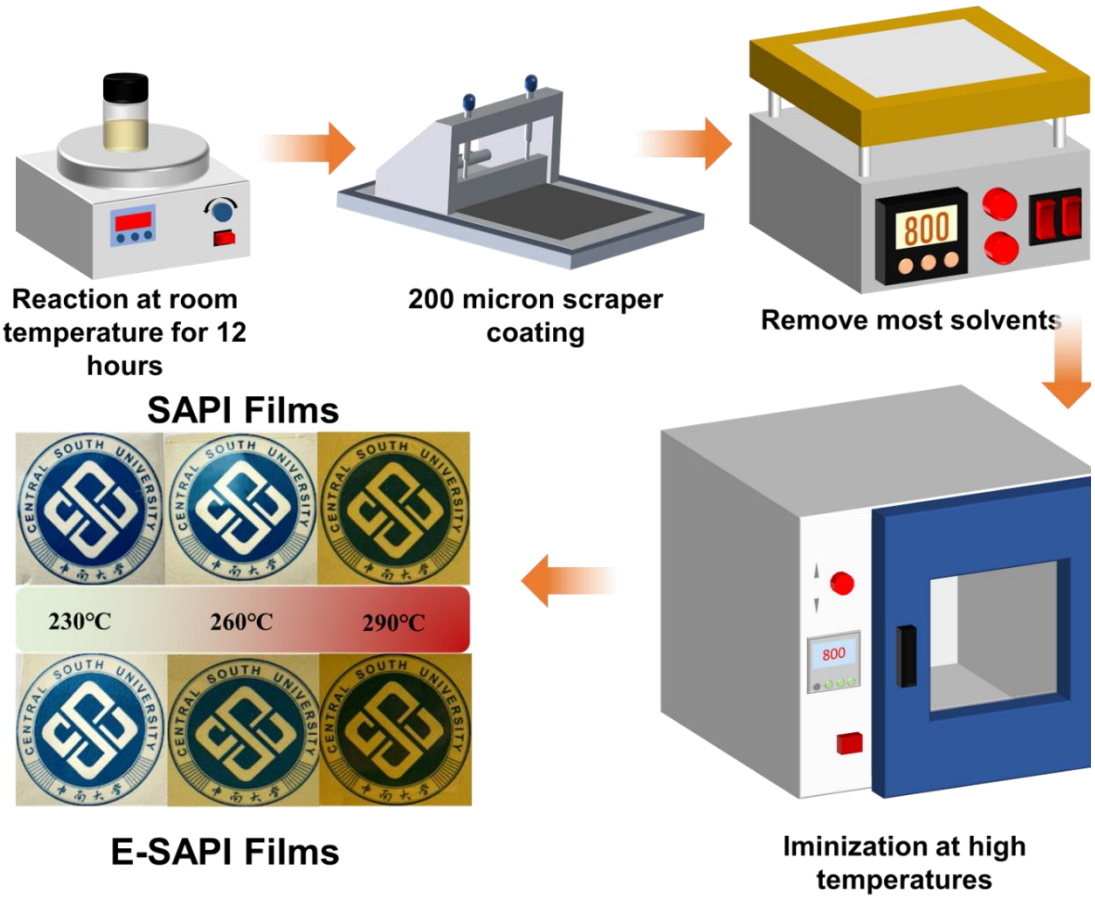

Figure S3. The preparation process of the film and the film under air at different temperatures.

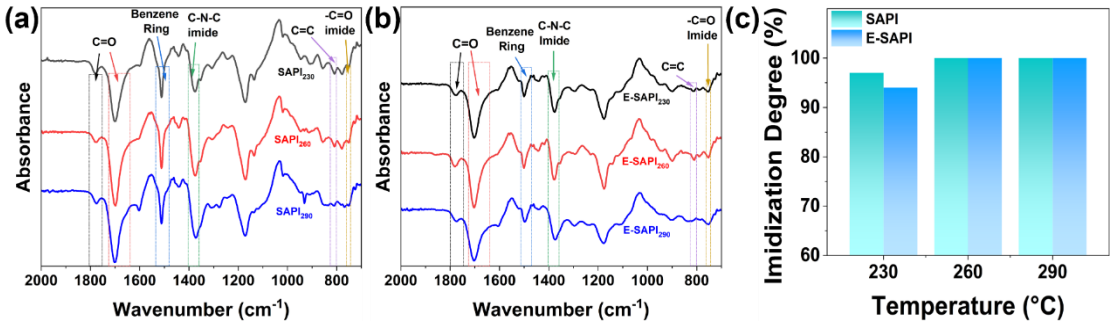

Figure S4. ATR-FTIR spectrum for (a) SAPI and (b) E-SAPI with different imidization temperatures. (c) Variation of imidization degree with different temperatures.

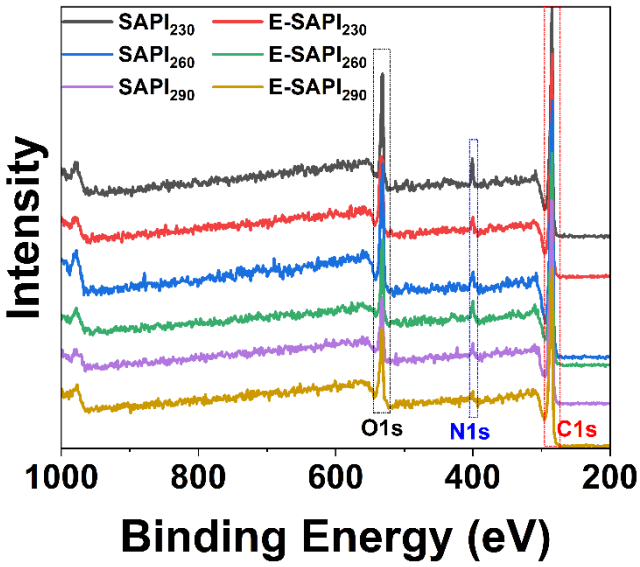

Figure S5. The XPS wide-scan spectra of SAPI and E-SAPI: C_{1s}, O_{1s} and N_{1s}.

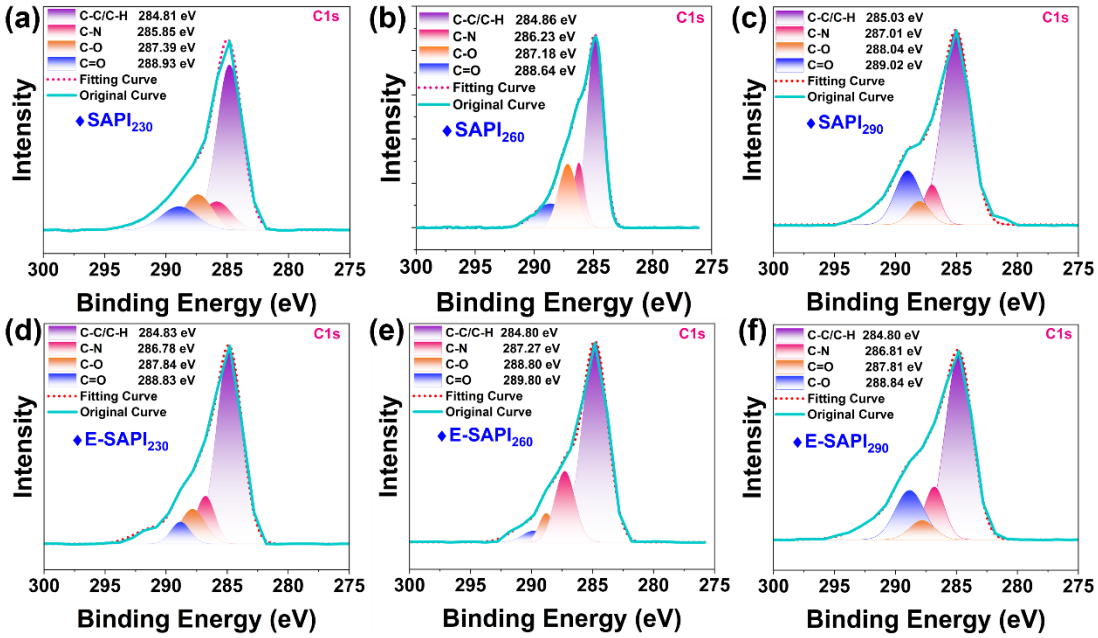

Figure S6. The C1s XPS spectrum of (a) $SAPI_{230}$, (b) $SAPI_{260}$, (c) $SAPI_{290}$, (d) E-$SAPI_{230}$, (e) E-$SAPI_{260}$ and (f) E-$SAPI_{290}$.

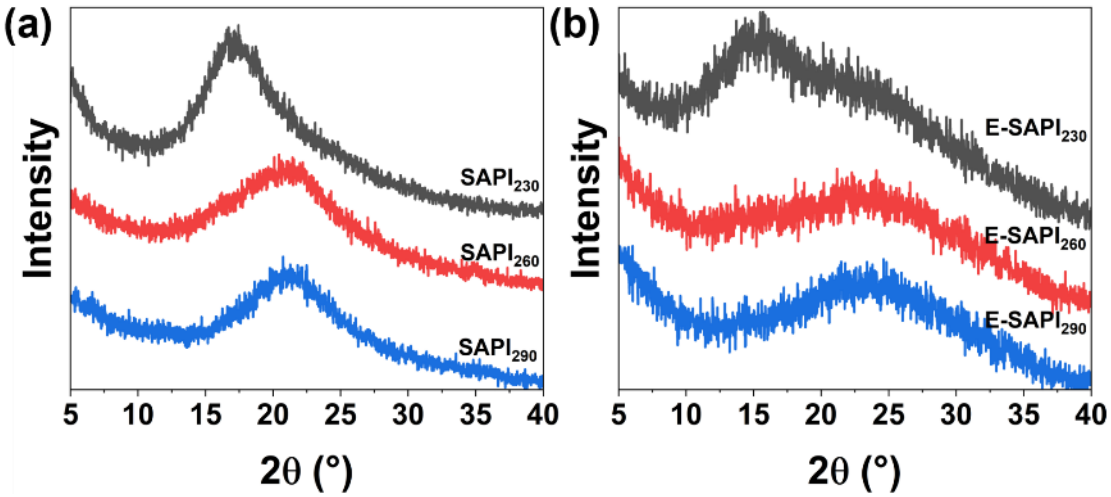

Figure S7. The XRD patterns of (a) SAPI and (b) E-SAPI.

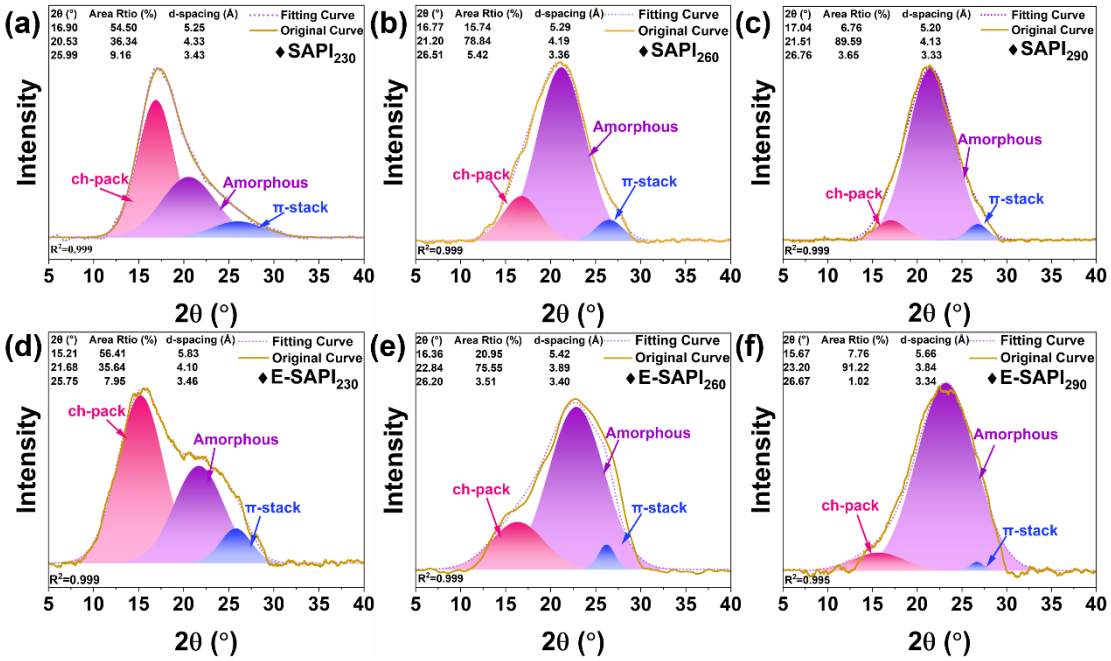

Figure S8. Multimodal fitting curves of XRD patterns of (a) $SAPI_{230}$, (b) $SAPI_{260}$, (c) $SAPI_{290}$, (d) $E\text{-}SAPI_{230}$, (e) $E\text{-}SAPI_{260}$ and (f) $E\text{-}SAPI_{290}$.

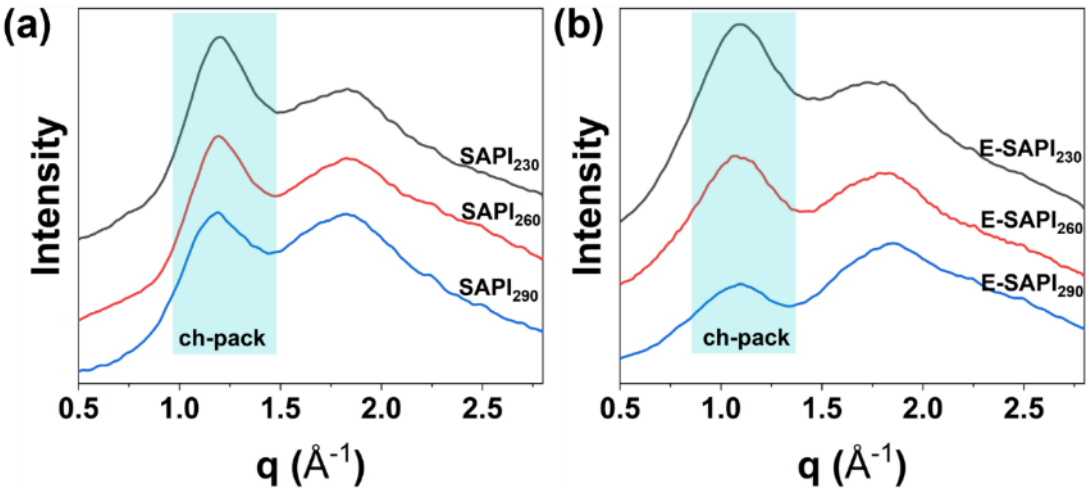

Figure S9. The WAXS patterns of (a) SAPI and (b) E-SAPI.

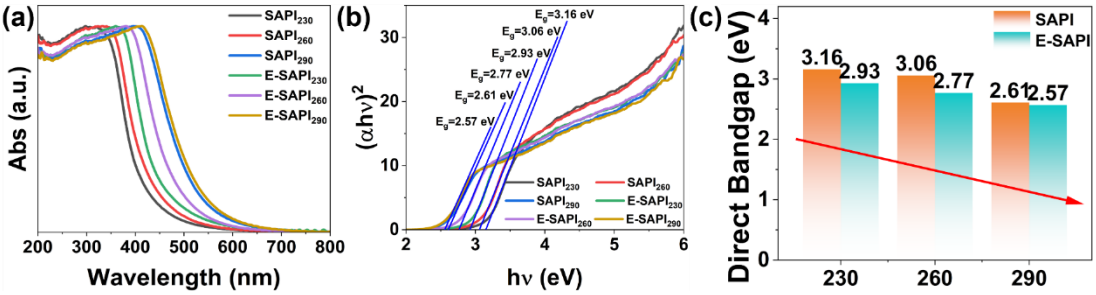

Figure S10. (a) The UV-vis absorption curves of SAPI and E-SAPI. (b) The optical E_g of SAPI and E-SAPI is calculated by UV-vis curves. (c) The optical E_g as a function of imidization temperature.

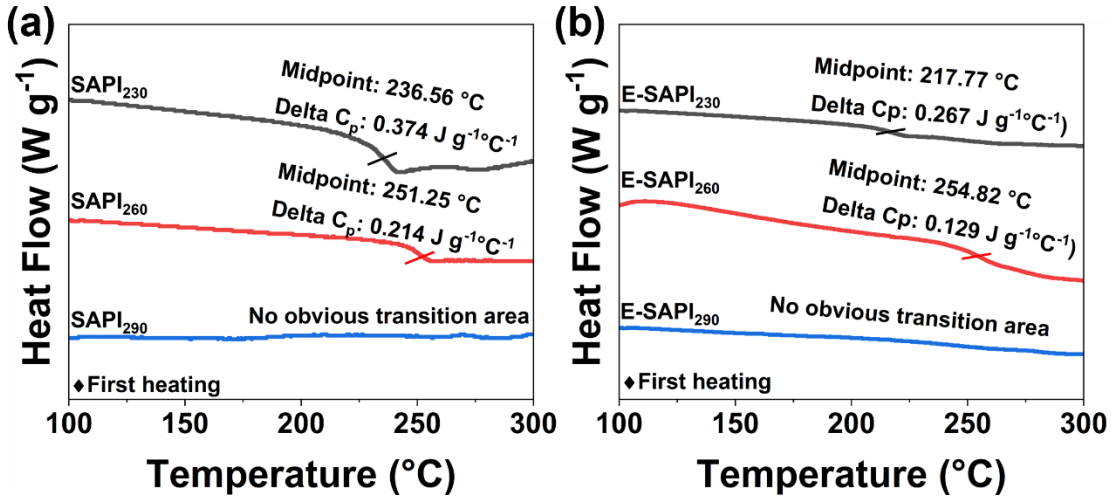

Figure S11.The DSC curves of (a) SAPI and (b) E-SAPI.

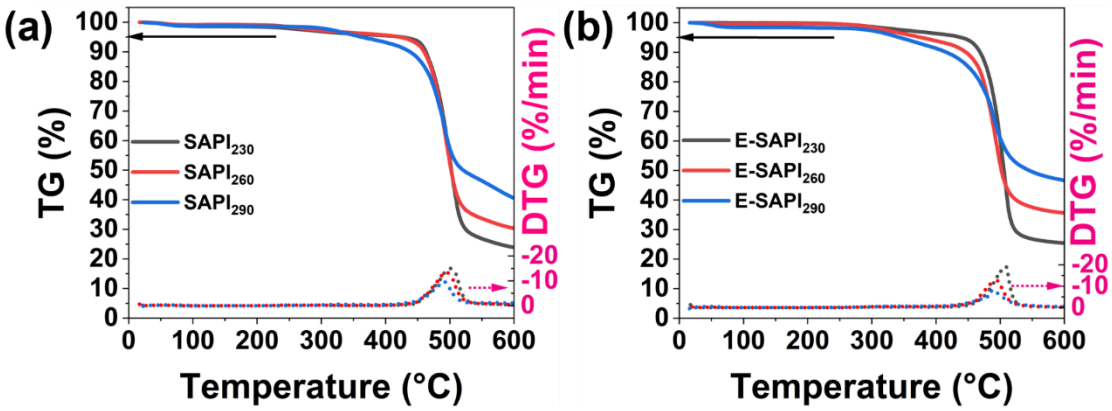

Figure S12.The TGA curves of (c) SAPI and (d) E-SAPI.

Figure S13. Solvation test of SAPI and E-SAPI films in N-methylpyrrolidone solvent.

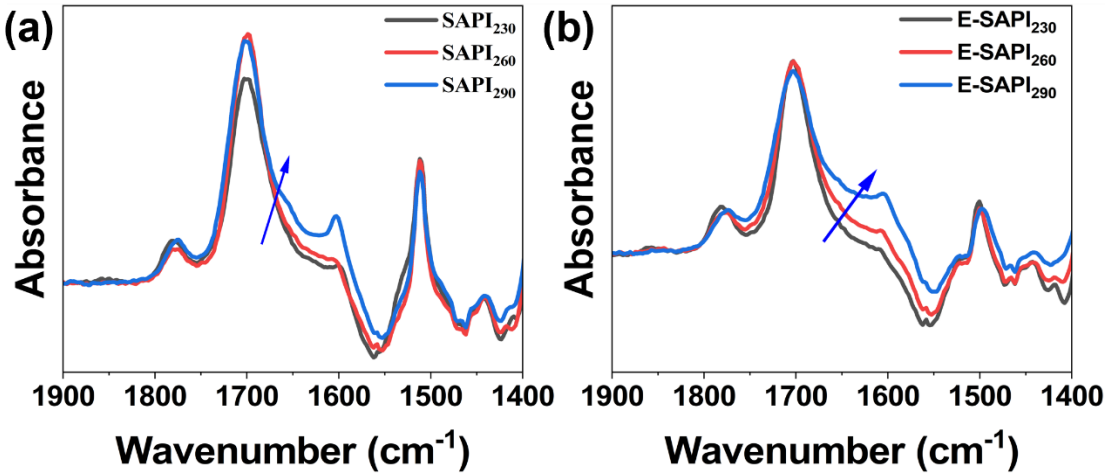

Figure S14. The ATR-FTIR spectra of SAPI and E-SAPI at 1400-1900 cm^{-1}.

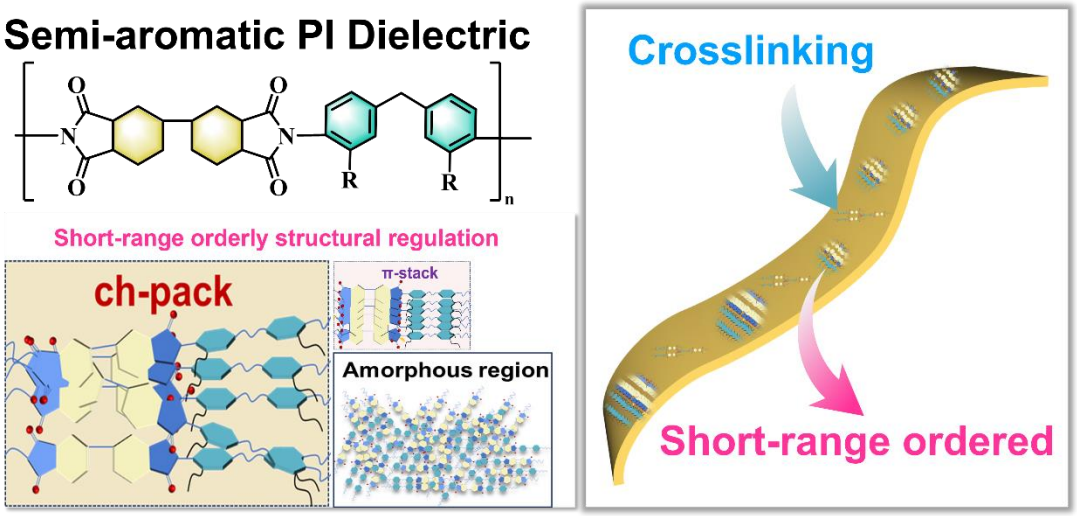

Figure S15. Schematic diagram of dual regulation of thin film properties by short-range ordered structure and crosslinked structure.

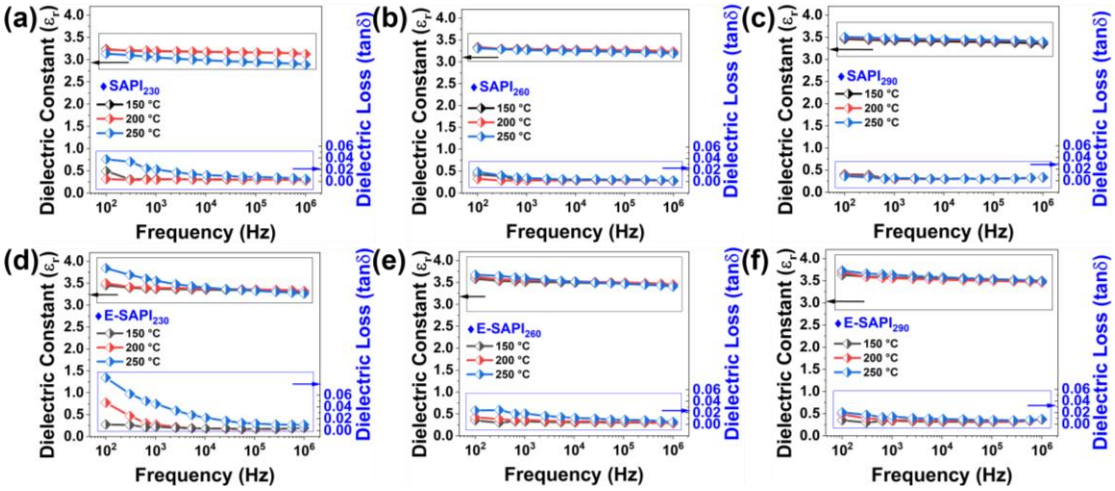

Figure S16. Dielectric temperature spectra of (a) $SAPI_{230}$, (b) $SAPI_{260}$, (c) $SAPI_{290}$, (d) E-$SAPI_{230}$, (e) E-$SAPI_{260}$ and (f) E-$SAPI_{290}$.

Figure S17. The images of dielectric films prepared under vacuum at different imidization temperatures.

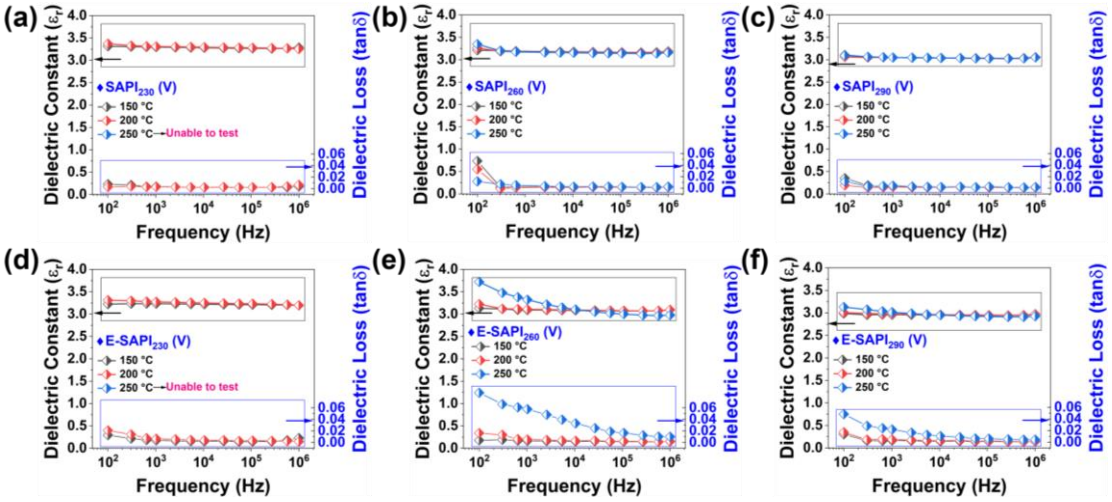

Figure S18. Dielectric temperature spectra of (a) $SAPI_{230}$ (V), (b) $SAPI_{260}$ (V), (c) $SAPI_{290}$ (V), (d) E-$SAPI_{230}$ (V), (e) E-$SAPI_{260}$ (V) and (f) E-$SAPI_{290}$ (V).

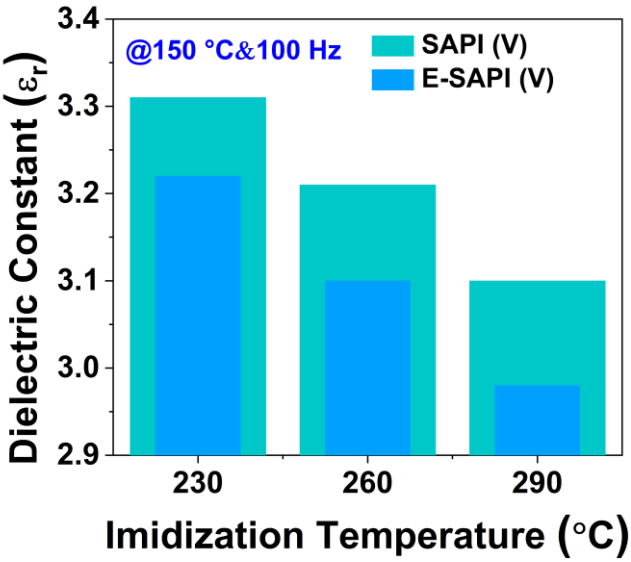

Figure S19. (d) The ε_r of $SAPI_{230}$ (V), $SAPI_{260}$ (V), $SAPI_{290}$ (V), E-$SAPI_{230}$ (V), E-$SAPI_{260}$ (V) and E-$SAPI_{290}$ (V) at 150 °C and 100 Hz.

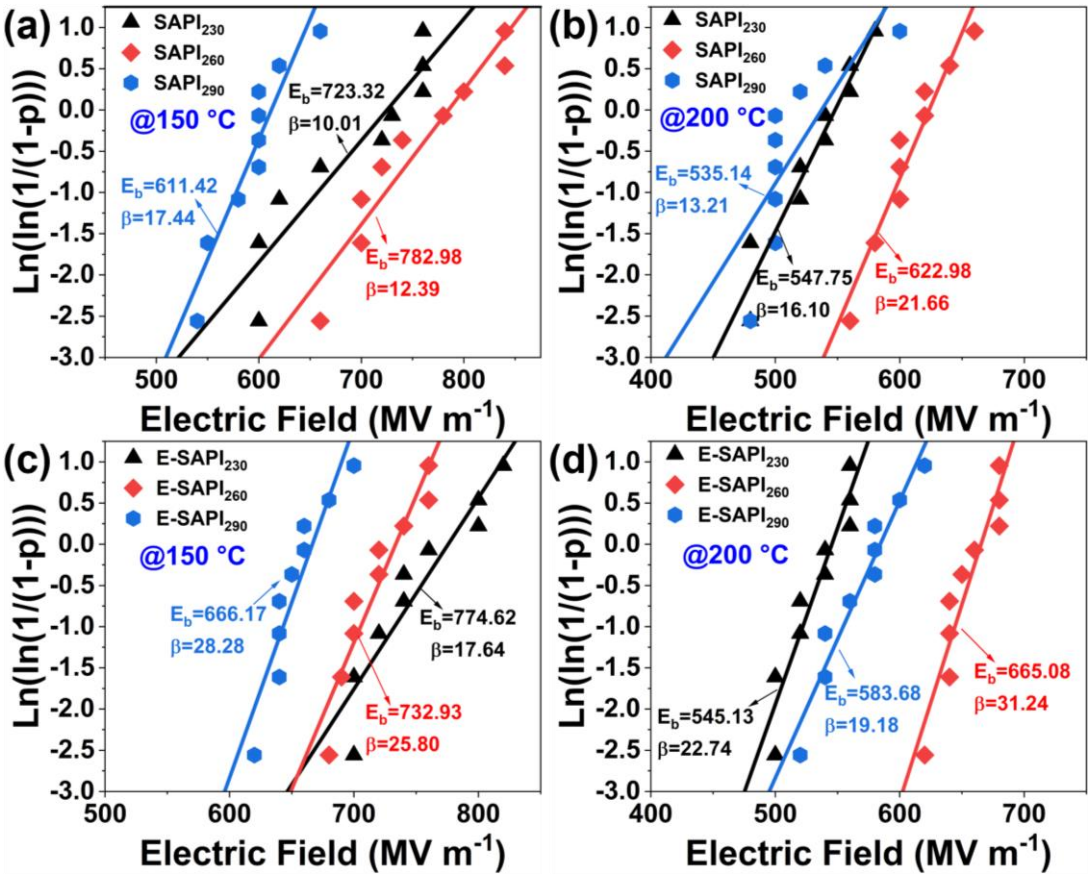

Figure S20. The Weibull curves of SAPI at (a) 150 ℃ and (b) 200 ℃. The Weibull curves of E-SAPI at (c) 150 ℃ and (d) 200 ℃.

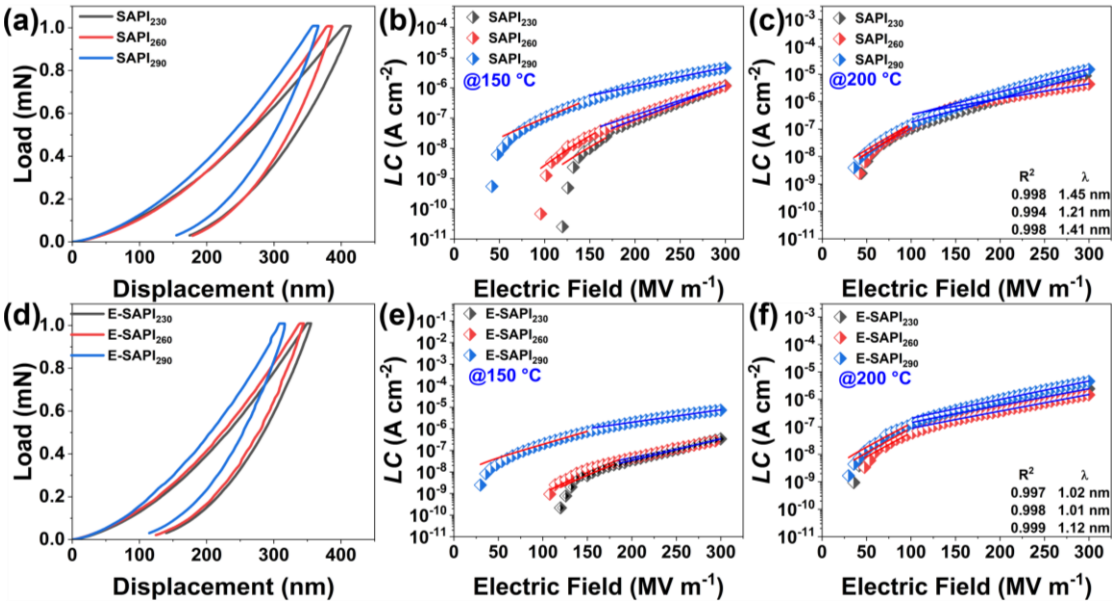

Figure S21. The load-displacement curve of (a) SAPI and (d) E-SAPI. The *LC* density of (b) SAPI and (e) E-SAPI at 150 ℃ and 100 Hz. The *LC* density of (c) SAPI and (f) E-SAPI at 200 °C and 100 Hz.

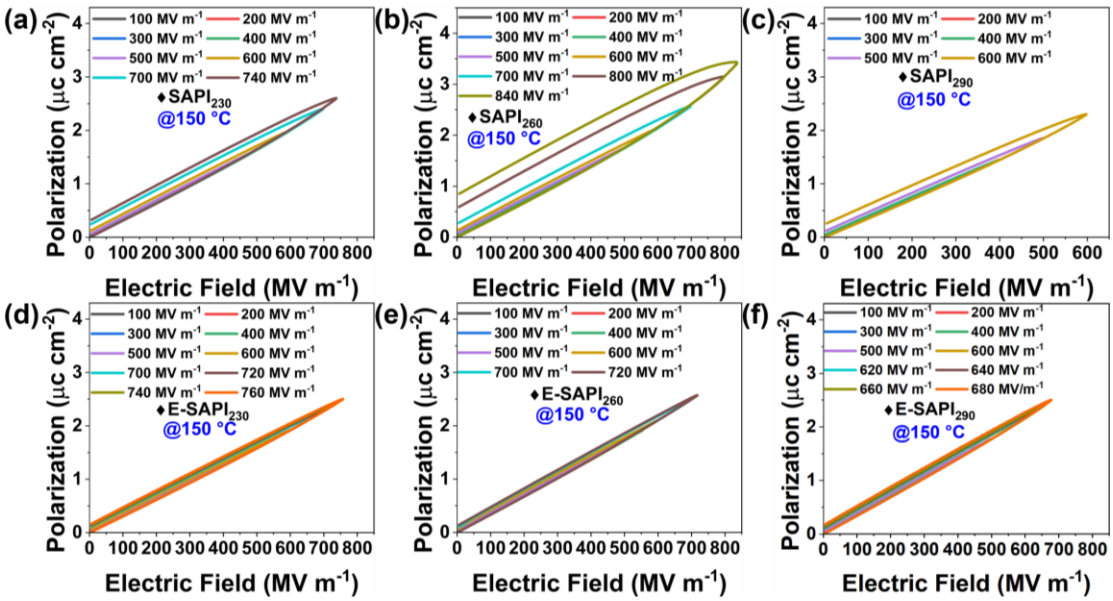

Figure S22. The P-E curves of (a) $SAPI_{230}$, (b) $SAPI_{260}$, (c) $SAPI_{290}$, (d) E-$SAPI_{230}$, (e) E-$SAPI_{260}$ and (f) E-$SAPI_{290}$ at 150 ℃ and 100 Hz.

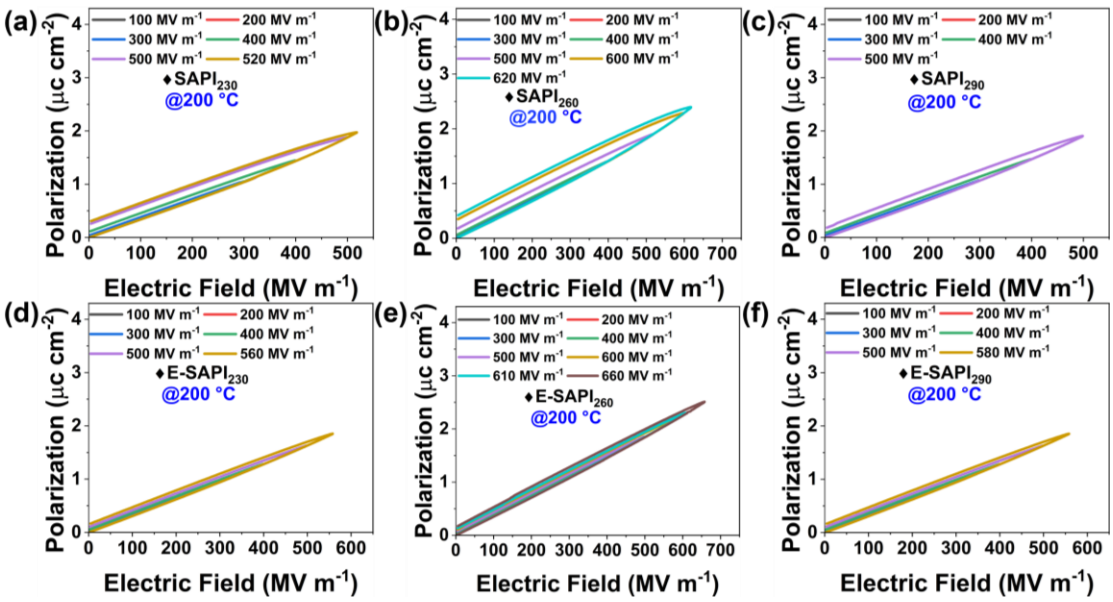

Figure S23. The P-E curves of (a) $SAPI_{230}$, (b) $SAPI_{260}$, (c) $SAPI_{290}$, (d) E-$SAPI_{230}$, (e) E-$SAPI_{260}$ and (f) E-$SAPI_{290}$ at 200 ℃ and 100 Hz under different imidization temperature.

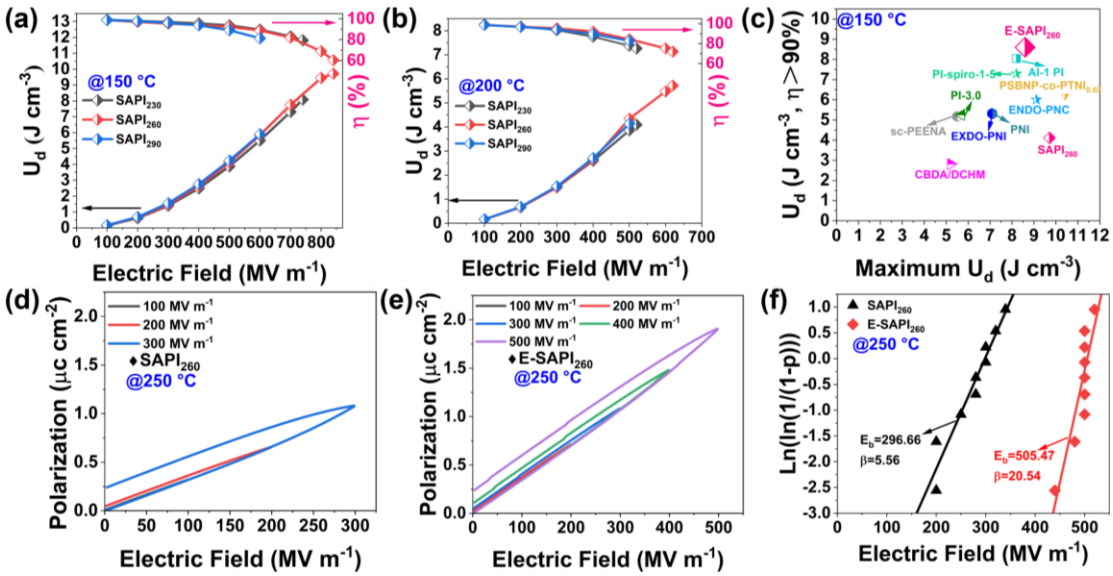

Figure S24. The U_d and η of SAPI at (a) 150 ℃ and (b) 200 ℃. (c) The maximum U_d and the U_d above 90% of all-organic dielectrics at 150 ℃ in the literature. (d) The P-E curves of (a) $SAPI_{260}$ and (b) E-$SAPI_{260}$ at 250 °C. (c) The Weibull curves of $SAPI_{260}$ and E-$SAPI_{260}$ at 250 °C.